EPJ manuscript No.
(will be inserted by the editor)

Gamma-ray flux measurement and geothechnical studies at the selected site for the LABChico underground laboratory

A. Aguilar-Arevalo[1], X. Bertou[2], C. Canet [3], M. A. Cruz[3], A. Deisting[4], A. Dias[4], J. C. D'Olivo[1], F. Favela-Pérez[1,2], E. A. Garcés[5a], E. González García[6], A. González Muñoz[5], J. O. Guerra-Pulido[1], J. Mancera-Alejandrez[6], D. J. Marín-Lámbarri[5b], A. M. Martínez Mendoza[5c], M. Martínez Montero[1], J. Monroe[4], S. Paling[7], S. Peeters[8], P. R. Scovell[7], C. Türkoğlu[8], I. G. Vallejo Castillo[6], E. Vázquez-Jáuregui[5d], and J. Walding[4]

[1] Instituto de Ciencias Nucleares, Universidad Nacional Autónoma de México, CDMX, Mexico
[2] Centro Atómico Bariloche, CNEA/CONICET/IB, Bariloche, Argentina
[3] Centro de Ciencias de la Atmósfera, Universidad Nacional Autónoma de México, CDMX, 04510 Mexico
[4] Royal Holloway, University of London, Egham Hill, United Kingdom
[5] Instituto de Física, Universidad Nacional Autónoma de México, A. P. 20-364, México D. F. 01000, Mexico
[6] Facultad de Ingeniería, Universidad Nacional Autónoma de México, Mexico
[7] Boulby Underground Laboratory, Boulby Mine, Saltburn-by-the-Sea, United Kingdom
[8] Department of Physics and Astronomy, University of Sussex, Brighton, United Kingdom

Received: date / Revised version: date

Abstract The γ-ray flux inside *La Guadalupe* mine, the selected site for the construction of the underground laboratory LABChico in Mexico, is reported for energies below 3 MeV. Data was recorded with a 0.669 kg thallium-activated sodium iodide (NaI) crystal detector deployed for 3.6 hr. The detector response was calculated via Monte Carlo simulations with GEANT4 and validated against point like calibration sources, and the γ-ray spectrum was extracted using an unfolding technique. The γ-ray flux above 250 keV and below 3 MeV is 0.1768 $\gamma/\mathrm{cm}^2/\mathrm{s}$. The two most intense γ-rays in the natural radioactive background, ^{40}K and ^{208}Tl, were identified. The flux measured for these isotopes is $0.0363 \pm 0.0020\,\gamma/\mathrm{cm}^2/\mathrm{s}$ and $0.0016 \pm 0.0005\,\gamma/\mathrm{cm}^2/\mathrm{s}$, respectively. A γ-ray spectrometry analysis of rock samples showed 597.60 ± 0.60 Bq/kg, 21.14 ± 0.03 Bq/kg, and 15.14 ± 0.05 Bq/kg of ^{40}K, ^{232}Th, and ^{238}U, respectively. These results are compared with deep underground facilities such as SURF, SNOLAB, Boulby, Modane, and Gran Sasso, with differences observed mainly due to the rock composition. Geotechnical studies of the mine and its rock composition are also reported.

1 Introduction

Underground laboratories [1, 2, 3, 4, 5, 6, 7, 8, 9, 10, 11, 12, 13] are fundamental physics research facilities in which astroparticle and nuclear physics experiments are constructed and operated. These experiments focus on leading questions within contemporary physics, such as the nature of the dark matter which pervades the Universe, the fundamental properties and nature of neutrinos, and their sources. The capabilities of such facilities extend to include a wide range of science topics, including environmental radioactivity, radio-assay, sub-surface life, mining, and geology [2, 3, 4, 5, 6, 7].

The development of techniques for rare event searches, and ultra-low radioactivity assay techniques is crucial for the success of the physics programs taking place in these facilities. The depth at which the laboratories are located is required to shield the experiments from cosmic radiation that bombards Earth's surface. Besides, environmental radioactivity from the surrounding rock and detector's components requires additional *in-situ* shielding to remove these backgrounds. A thorough determination and characterization of the natural radioactivity background flux are required [14, 15, 16, 17, 18, 16, 19, 20, 21, 22] to successfully achieve a low background environment. This is usually measured with γ-ray radiation detection systems, such as Ge and NaI crystals. Natural radioactivity from the decay

[a] egarces@fisica.unam.mx
[b] marinlambarri@gmail.com
[c] miichmtz@ciencias.unam.mx
[d] ericvj@fisica.unam.mx

of primordial radionuclides (^{40}K, ^{235,238}U, and ^{232}Th) is the main source of background radiation. These isotopes are present in the rock surrounding the tunnels and caverns of the laboratories. The actinium, uranium, and thorium series, the three natural decay series, have as parents the ^{235,238}U and ^{232}Th isotopes, respectively. Each series comprise many decay products, through the consecutive disintegration of the primordial radionuclide [23]. With a NaI detector it is possible to determine the uranium and thorium abundance through γ-ray assay by detecting the 1.76 MeV and 2.61 MeV γ-rays emitted by the ^{214}Bi and ^{208}Tl isotopes, respectively. The potassium abundance can be determined by detecting the 1.46 MeV γ-ray in ^{40}K decay.

The first underground laboratory in Mexico, Laboratorio Subterráneo de Mineral del Chico (LABChico), will be located in a decommissioned mine named *La Guadalupe* (20°13'11.52"N, 98°44'10.43"W), one of two decommissioned mines in the *Minas Rio El Milagro* geosite, listed among the sites of geological and cultural interest of the Comarca Minera UNESCO Global Geopark, Hidalgo State, Mexico [24, 25, 26]. The selected site in which the laboratory will be constructed is surrounded by approximately 100 m of rock, 300 m.w.e. (meter water equivalent) overburden. LABChico is focused on the development of research and educational programs through the establishment of a γ-ray assay facility initially consisting of two High Purity Germanium detectors [27]. A dedicated program in fundamental and applied science is devised, where γ-ray assay of detector components for underground astroparticle physics will be developed, in addition to environmental radiation monitoring applications, see [2, 3, 4, 5, 6, 7, 8].

In this work we report on the measurement of γ-ray fluxes for primordial radionuclides in the LABChico site, measured with a thallium-activated sodium iodide (NaI) crystal detector. Geotechnical studies are also relevant for the construction of the laboratory and for modifications (i.e., excavations) to the tunnel to accommodate the projected laboratory usable space; however, compromise has to be made to preserve the historical mining heritage of the site, following the UNESCO geoparks recommendations [24].

Geotechnical studies, presented here, are needed to have a compelling notion of the mine morphology and topography, in order to find the optimal location for the laboratory construction, these studies provided important information about the maximal rock coverage place where a major muon flux absorption is expected. The geotechnical studies campaign allowed the procurement of rock samples. The samples were radio assayed to determine the concentration of radio-isotopes contributing to the environmental background radiation measurement described in this work.

This paper is organized as follows. Section 2 describes the NaI detector and its characterization, section 3 reports the γ-ray background flux measurement, section 4 shows the results discussion and a comparison of measurements in other underground laboratories along with the rock samples radio assay results and section 5 describes the site geotechnical studies. The conclusions are presented in section 6.

2 NaI Detector

A 0.669 kg thallium-activated NaI crystal detector was commissioned for the γ-ray background flux measurement at a location in the tunnel leading to the selected LABChico site, see label 2 in Fig. 1. This detector is property of the Neutrino and Dark Matter Laboratory at the Institute of Physics at the National Autonomous University of Mexico (UNAM). The detector, model SDA-38 [28], manufactured by Spectrum Techniques, was used along with a data acquisition system (DAQ), consisting of a universal computer spectrometer (UCS-30) with an internal bipolar preamplifier, including polarity selection as well as multiple shaping times with up to 4096 channels of conversion gain.

The detector dimensions were obtained from the technical sheet provided by the manufacturer [28], listed below and shown in Fig. 2:

1. **NaI crystal**: cylindrical solid sodium iodide (thallium-activated), 38.1 mm diameter, and 152.4 mm length, with a centered cubic face.
2. **Housing**: a stainless steel cover, in which the crystal is enclosed, with 44.5 mm diameter, and 168.3 mm length.
3. **Optical interface**: the crystal is also enclosed by a Rexon RX-22C (Al203 glass) optical interface.
4. **Spring**: attached to one of the sides of the stainless steel jacket, to dampen the movement of the interior components.
5. **Optical window**: the crystal is in contact with a pyrex optical window coupling to the photomultiplier tube (PMT).
6. **PMT B76B01**: photomultiplier tube manufactured by Ortec, attached to the optical window.

A set of pointlike sources [29] was used to perform the energy calibration and validate the linear response of the detector. The detector dimensionless energy resolution is defined as the ratio $R = \mathrm{FWHM}/E$, where the full width

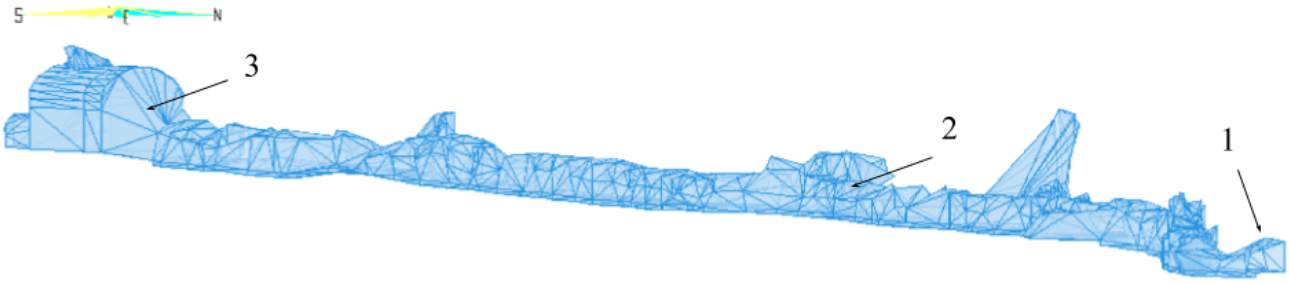

Figure 1: Three-dimensional model of the tunnel of *La Guadalupe* mine depicting the original geometry as obtained from the topographic surveys. (1) Mine entrance, (2) Location of the γ-ray background flux measurement (45 m away from the entrance) and (3) Site for the construction of the laboratory (150 m away from the entrance, with a surface of approximately 25 m^2).

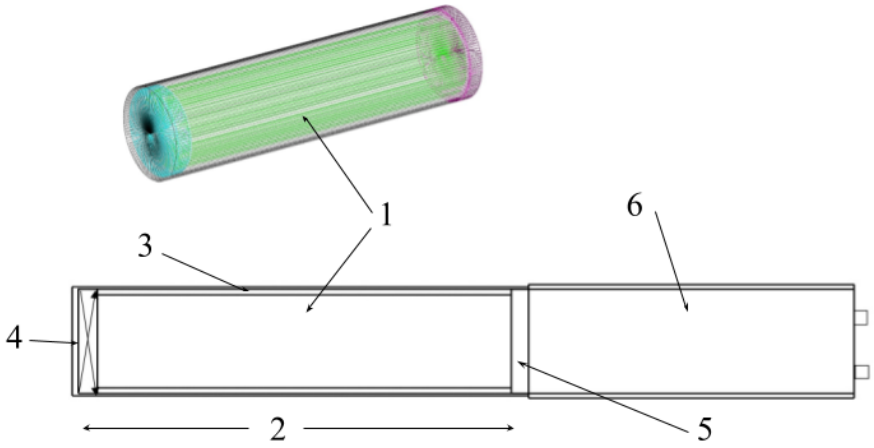

Figure 2: Top figure shows the GEANT4 detector geometry and bottom figure a schematic representation of the NaI detector and its components. 1) NaI crystal, 2) Housing, 3) Optical interface, 4) Spring, 5) Optical window and 6) PMT.

at half maximum is FWHM $= 2\sqrt{2\ln 2} \times \sigma \simeq 2.355\sigma$ and σ [keV] the standard deviation parameter from a Gaussian fit to the photo-peak. E is the energy (central value) of the photo-peak. The standard deviations measured with the ^{137}Cs and ^{60}Co sources are 20.2 $\pm$ 0.3 keV at 662 keV and 26.3 $\pm$ 0.9 keV at 1.33 MeV, equivalent to 7 % and 5 % FWHM, respectively. The value measured at 662 keV is in agreement within a few percent to the one reported by the manufacturer of 8.5 % FWHM, equivalent to σ = 23.9 keV [28]. Fig. 3 shows the energy resolution of the crystal as function of the energy measured with the ^{57}Co, ^{22}Na, ^{137}Cs, and ^{60}Co pointlike sources.

2.1 Monte Carlo Validation

The γ-ray detection was simulated using the toolkit GEANT4 version 10.01.p03 [30]. The components listed in section 2 and the dimensions and properties of the materials, such as density and chemical composition, were included in the simulation, excluding the PMT. This last component was not included since the simulations only take into account the energy deposition in the NaI crystal.

The γ-ray emission from pointlike sources ^{22}Na, ^{137}Cs, and ^{60}Co [29] was simulated, computing full-energy peak efficiencies of the simulated detector and then compared with experimental data. These sources have an initial activity (January 2019) of 1 μCi, except for ^{137}Cs (0.1 μCi), with a reported activity uncertainty of 20 %.

The measurement was performed placing the detector and sources inside a cylindrical lead shield (8.89 cm outer diameter, 4.45 cm inner diameter, and 6.35 cm height). Each source was placed 2 cm away from the detectors front side. The sources were simulated as ions with the GEANT4 General Particle Source and their γ-ray emissions as decays with the

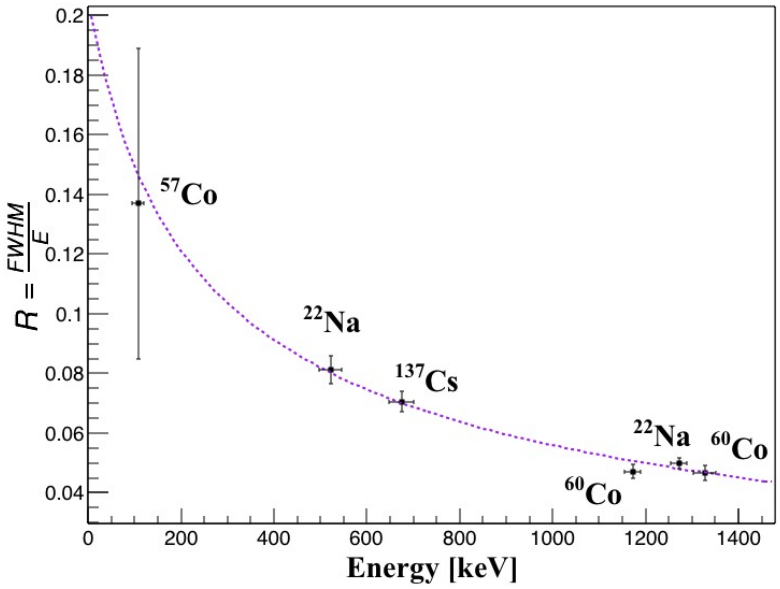

Figure 3: Resolution for the NaI detector as a function of the γ-ray energy for pointlike calibration sources. The magenta dashed line represents the fit to the empirical function $R = \frac{[P_0]}{\sqrt{[P_1]+E}} + [P_2]$, where the parameter values P_0=2.57 $\pm$ 1.14 keV$^{1/2}$, P_1=129.10 $\pm$ 256.20 keV and P_2= -0.020 $\pm$ 0.025. Errors in σ and E were increased by a factor χ^2/n.d.f given by the fit to account for non-Gaussianities in the measured photopeaks for χ^2/n.d.f > 1.

Radioactive Decay Module [31]. The deposited energy in the NaI crystal was calculated adding up the energy deposited by all the secondary particles, produced through ionization processes by the primary γ-ray. Then the information was stored in ROOT files [32].

The NaI detector was positioned in its vertical configuration for the data acquisition, using the scintillation stand with sample tray (SPA38 Spectrum Techniques) [28]. Independent measurements for each source were taken with the same configuration as in the simulation. A voltage bias of 700 V was applied to the detector for each γ-ray source measurement.

The full-energy peak efficiency, for the experimental and simulated data, was computed as the ratio of detected to the total γ-ray emissions, using the following equation:

$$\epsilon = \frac{N_F}{P_\gamma N_T}, \tag{1}$$

where N_F corresponds to the full-energy peak count rate (in counts per second), P_γ is the emission probability of the specific γ-ray being measured (the ratio of γ-ray emissions per second for a specific energy and the total number of isotope disintegrations, taken from [33]), and N_T is the total number of γ-rays emitted at the specific energy which was corrected for decay using the radioactive decay law and the originally reported activity at the source preparation date.

The full-energy peak count rate N_F is obtained by fitting the spectrum to a Gaussian plus an order one polynomial, counting the total rate in a 3 standard deviations range about the mean and subtracting the event rate under the fitted polynomial that models the background [32], see Fig. 4 as an example for the ^{137}Cs spectrum. The percent difference among experimental and simulated full-energy peak efficiencies, $(\epsilon_{MC} - \epsilon_{Data})/\epsilon_{MC}$, at 1.33 MeV, the highest energy available, is 6 %.

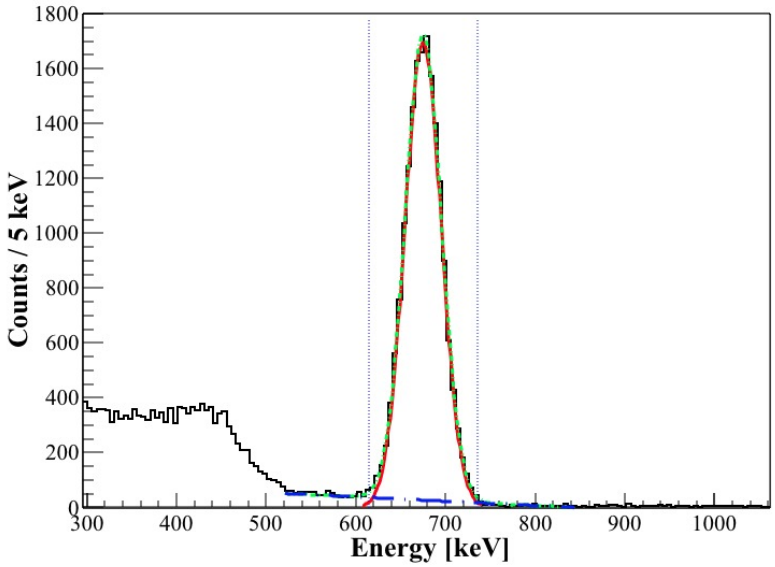

Figure 4: Caesium-137 calibrated spectrum. The peak count rate is determined subtracting the linear background (blue line) fitted simultaneously with a Gaussian (red line) to the total number of counts in the 3 sigma range about the mean. The green dotted line shows the fitted function (Gaussian plus order one polynomial).

3 Gamma-Ray Background Flux Measurement

3.1 Data acquisition

The experimental setup inside the mine, including the detector, electronics, DAQ system, and computer, was positioned 45 m away from the mine entrance as shown in Fig. 1. A petrol generator was used as a power supply and was left outside the tunnel for safety considerations. The experimental components were enclosed in two acrylic boxes (50 $\times$ 50 $\times$ 50 cm) to avoid the humidity present in the mine (see Fig. 5). One of the boxes contained the electronics, DAQ system, and computer, and the other, the NaI detector. A total of 12907.56 s (3.6 hr) of data were taken with a 750 V bias voltage applied to the detector.

Fig. 6 (blue line) shows the γ-ray spectrum measured inside the mine. Two characteristic peaks from isotopes present in the rock were identified (^{40}K at 1.46 MeV, and ^{208}Tl at 2.61 MeV). The detector energy calibration was performed using the natural background ^{40}K and ^{208}Tl photopeaks with a resolution of 8.7 % (σ = 54 keV) and 6% (σ = 66 keV), respectively.

Each photopeak was fitted to a Gaussian function plus an order one polynomial, using ROOT analysis tools [32]. The Gaussian mean fit parameter is the channel number associated to the γ-ray energy and its standard deviation σ is related to the detector resolution at the given energy. The order one polynomial corresponding to the fitted background is subtracted from the total number of counts in a three σ range about the mean and the correspondence between the γ-ray energy and channel number is obtained (energy calibration).

3.2 Gamma-ray spectrum unfolding

The γ-ray background flux measurement with the NaI detector inside the mine is shown in Fig. 6, (blue line). As the main concern is to extract the net γ flux, rather than reconstructing the detailed shape of the spectrum, the measured data was rebinned into six coarse bins, significantly reducing the statistical uncertainties and allowing to directly apply the unfolding procedure of inverting the response matrix. The measured flux Φ_{Exp} is related to the actual γ-ray background flux Φ_{True} in the environment [34], through the detector response matrix $\mathbf{R}$:

$$\Phi_{Exp} = \mathbf{R}\Phi_{True}. \tag{2}$$

The detector response matrix, $\mathbf{R}$ in the above equation, is calculated using Monte Carlo simulations [31]. In the GEANT4 geometry, the detector (described in section 2.1) was placed inside an acrylic box of 50 $\times$ 50 $\times$ 50 cm, and

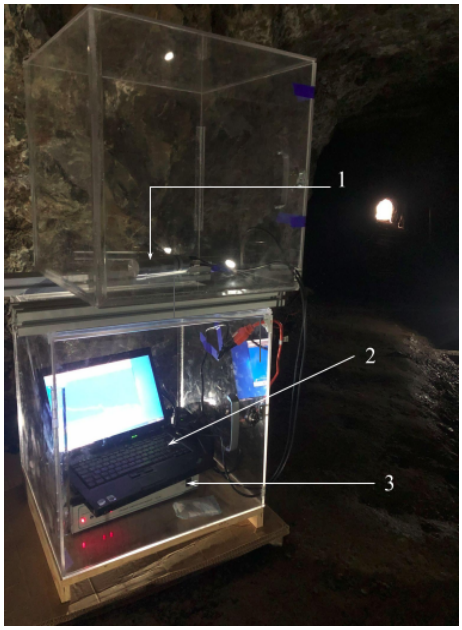

Figure 5: Photo of the experimental setup inside the mine (45 m from the entrance). The detector (1) is enclosed by an acrylic box (top box), and the computer (2) and the DAQ system (3) are inside the bottom acrylic box.

6 mm thick. The simulated setup was placed in the center of a shell, made of concrete *, 10 cm thick with an inner radius of 1 m. Gamma-rays were randomly generated from the inner surface of the shell, pointing to the NaI crystal center, and propagated through air before reaching the detector.

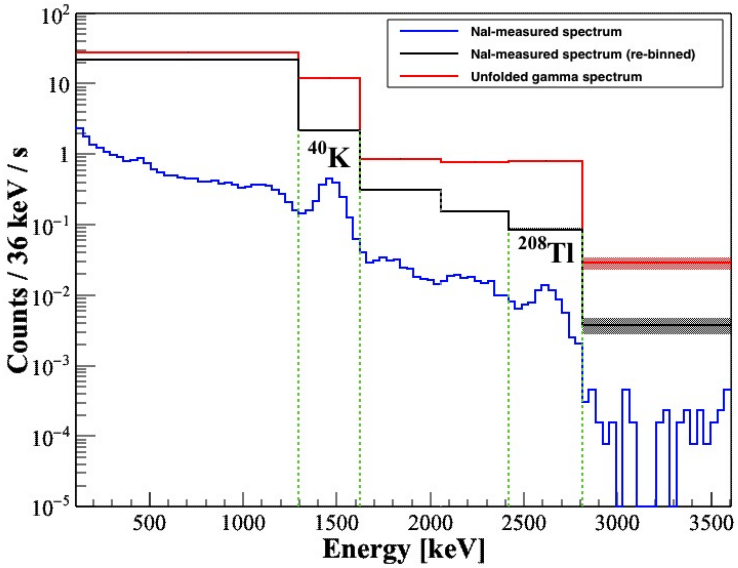

Figure 6: Blue line, γ-ray background spectrum measured inside *La Guadalupe* mine. Black line, the spectrum re-binned into the chosen energy ranges for the unfolding procedure, Φ_{Exp} in equation 2. Red line, the calculated unfolded spectrum Φ_{True} in equation 2. Vertical green lines, ranges corresponding to ^{40}K and ^{208}Tl.

*The choice of the material is irrelevant, as scattering effects from the cavern wall are negligible.

The energy range for the simulations required for the response matrix calculation was based on the experimental data taken in the mine, where two peaks were identified in the range from 100 to 3064 keV, corresponding to the primordial isotopes emissions of ^{40}K and ^{208}Tl (see Fig. 6).

The center of these peaks is identified using Gaussian fits. Then, the whole energy range is divided into six energy bins, as shown in table 1. For each energy bin, γ-rays were generated randomly between the limits of the bin following a flat distribution, and the information was stored in ROOT files.
Each entry in the response matrix $\mathbf{R}$ (Eq. 3), is calculated as the ratio of the number of simulated events in bin j of reconstructed energy E_{Rec}, to the total number of events simulated in bin i of the true energy E_{True}. $R_{i,j}$ is the efficiency in the response matrix to observe events with a given reconstructed energy, given that they have a given true energy E_{True}. Entries below the diagonal are zero since it is expected that events from the lower energy bin do not add counts to a higher energy bin.

$$\mathbf{R} = \begin{bmatrix} 6.040 & 3.600 & 2.620 & 1.860 & 1.420 & 1.090 \\ 0 & 1.690 & 0.998 & 0.728 & 0.532 & 0.298 \\ 0 & 0 & 1.480 & 1.200 & 0.977 & 0.539 \\ 0 & 0 & 0 & 1.160 & 0.931 & 0.696 \\ 0 & 0 & 0 & 0 & 1.040 & 0.943 \\ 0 & 0 & 0 & 0 & 0 & 1.300 \end{bmatrix} \times 10^{-1} \tag{3}$$

Energy bin keV	rate counts/s	rate unfolded counts/s	isotope -	isotope rate γ/cm^2/s
100-1298	22.274 ± 0.040	28.376 ± 0.027	-	-
1298-1622	2.193 ± 0.010	11.789 ± 0.080	^{40}K	0.0363 ± 0.0020 ± 0.0110
1622-2055	0.319 ± 0.010	1.042 ± 0.031	-	-
2055-2415	0.158 ± 0.004	0.706 ± 0.017	-	-
2415-2811	0.087 ± 0.003	0.774 ± 0.031	^{208}Tl	0.0016 ± 0.0005 ± 0.0005
2811-3604	0.004 ± 0.001	0.061 ± 0.006	-	-

Table 1: Gamma-ray rates per energy bin before and after the unfolding. The contribution from the identified isotopes ^{40}K and ^{208}Tl is also shown with their statistical and systematical uncertainties.

The inverse of the response matrix multiplied by the rebinned measured event rate gives the unfolded event rate per bin, see the black line and red line in Fig. 6, respectively. Peak event rate contributions from the isotopes ^{40}K and ^{208}Tl, were obtained following the method explained in section 2.1 for pointlike sources, where the original spectrum is fitted in the corresponding energy bin to a Gaussian function plus an order one polynomial and the integral under the polynomial is subtracted to the total event rate. From this procedure and assuming that the fraction of peak to background events remains constant in the unfolded spectrum Φ_{True}, the ^{40}K and ^{208}Tl isotopes contribution to the background flux is obtained as reported in the last column of table 1.

The total statistical uncertainty in the flux contributions includes: the uncertainty in the background event rate from the fit, exposure time, detector dimensions, and final isotope fraction (highest contribution). Statistical uncertainties in the calculations of the LABChico fluxes, last column in table 1, are in the order of 5.5 % for ^{40}K and 31 % for ^{208}Tl, and a systematical uncertainty of 30 % and 31 %, respectively, is included due to the 20 % uncertainty in the pointlike sources used for the Monte Carlo validation, which affects the efficiency values in the response matrix calculation used in the unfolding procedure.

4 Results and discussion

The design of shielding for low background counting experiments is driven by the γ-ray flux intensity measured in the underground facilities. The γ-ray background flux measured in LABChico (*La Guadalupe*) is similar to other underground facilities, since the flux below 3 MeV depends on the surrounding materials and rock composition but not on the depth. Measurement campaigns have been performed in SURF (Davis cavern) [15, 22], SNOLAB [14], Boulby [17], Modane [20], and Gran Sasso [16]. The measurement in LABChico is compared with the average value of the locations reported in each underground laboratory, when more than one location value is reported.

Table 2 shows a comparison of the γ-ray background flux for the ^{40}K and ^{208}Tl photopeaks with measurements in the SURF, SNOLAB, Boulby, Modane, and Gran Sasso underground laboratories. The γ-ray background flux for these primordial isotopes decreases as the energy range increases, as expected.

	Flux (γ/cm^2/s)	
Laboratory	^{40}K	^{208}Tl(^{232}Th)
LABChico	0.0363	0.0016
SURF (Davis cavern)	<0.3600	<0.0560
SNOLAB	0.0590	0.0160
Boulby	0.0027	0.0001
Modane	0.0030	0.0007
Gran Sasso	0.0020	0.0004

Table 2: Comparison of γ-ray background flux measurements for the ^{40}K and ^{208}Tl peaks for LABChico (*La Guadalupe*), SURF [14], SNOLAB [15], Boulby [17], Modane [20], and Gran Sasso [16].

Table 3 shows a comparison of the total background flux (between 250.2 and 2734.2 keV) and the flux for different energy ranges in *La Guadalupe* mine and the other underground laboratories. The flux from 250.2 to 2734.2 keV in *La Guadalupe* mine is similar to that of the other laboratories, with differences observed in the ^{40}K and ^{208}Tl energy ranges, whose intensity depends on the rock composition. Most of the fluxes reported in the different locations at Modane and Gran Sasso show variations from the average of approximately 35 % and 50 %, respectively.

	Flux (γ/cm^2/s)					
Range (keV)	250.2-500.4	500.8-1005.8	1005.6-1555.8	1556.2-2055.8	2056.2-2734.2	Total
LABChico	0.0331	0.0406	0.0871	0.0061	0.0080	0.1750
Boulby	0.0215	0.0163	0.0110	0.0714	0.0006	0.1208
Modane	0.0813	0.0561	0.0269	0.0065	0.0037	0.1745
Gran Sasso	0.0437	0.0308	0.0347	0.0035	0.0020	0.1147

Table 3: Comparison of γ-ray background flux in different energy intervals and the total integrated flux for LABChico (uncertainties are below 2.5 %) and the Boulby [17], Modane [20], and Gran Sasso [16]) underground laboratories (no uncertainties are reported).

The difference in the total integrated background flux, mostly due to the ^{40}K line, could be attributed to the rock composition in the laboratories and the lack of a concrete layer in LABChico, where the experimental facility is planned to start construction this year. Rhyolite and andesite, the most abundant rock types in *La Guadalupe* mine, show a high potassium concentration, alike SURF (rhyolite) and SNOLAB (norite). Boulby (halite and mudstone), Modane (calcschist), and Gran Sasso (dolomitic limestone) have lower potassium, uranium and thorium concentrations [17, 20, 16, 14].

Rhyolite is the most abundant rock type in the Davis cavern at Sanford Underground research Facility (SURF). Results reported by D. S. Akerib et. al [22], showed that rhyolite has a high ^{40}K activity in the cavern. A γ-ray flux of 0.35 $\pm$ 0.08 γ/cm^2/s from 1 to 3 MeV is reported, higher than the one measured in LABChico (see table 4 and Figure 7). Furthermore, SNOLAB also shows a high γ-ray flux, 0.23 $\pm$ 0.02 γ/cm^2/s from 1 to 3 MeV, but with a different rock type (norite) which also has a high potassium content.

	Flux	(γ/cm^2/s)	
Range (keV)	1000-2000	2000-3000	1000-3000
LABChico	0.09	0.01	0.10
SURF (Davis cavern)	0.30	0.05	0.35
SNOLAB	0.20	0.03	0.23

Table 4: Comparison of γ-ray background flux measurements from 1000 to 3000 keV among LABChico (uncertainties around 30 %), SURF (Davis Cavern), and SNOLAB, with reported uncertainties of up to 25 % and 10 %, respectively.

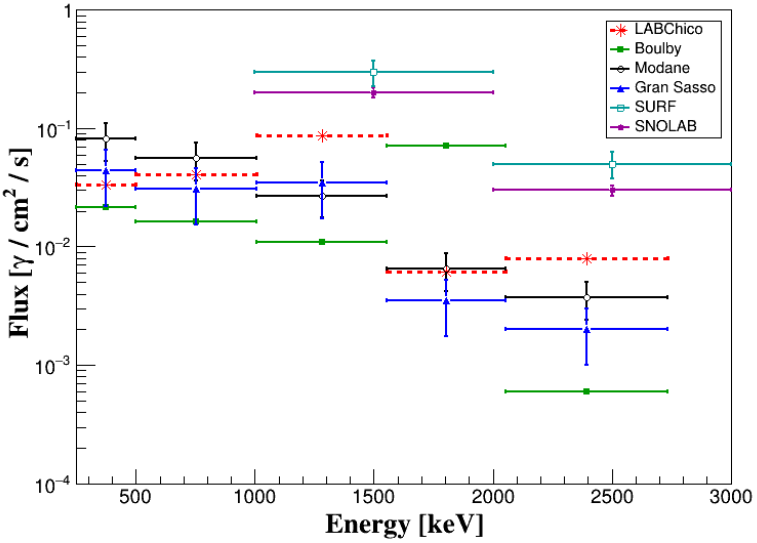

Figure 7: Comparison of γ-ray background flux in different energy intervals for LABChico (uncertainties are below 2.5 %) Boulby [17], Modane [20], Gran Sasso [16], SURF (Davis Cavern), and SNOLAB. Modane and Gran Sasso show variations from the average of approximately 35 % and 50 %, while SURF and SNOLAB report uncertainties of up to 25 % and 10 %, respectively.

4.1 Germanium detector rock sample analysis

During the geotechnical studies campaign, rock samples were extracted from *La Guadalupe* mine, crushed with a mill, placed into 240 ml Cole-Parmer wide-mouth sample containers, and measured in the Boulby Underground Germanium Suite (BUGS) [8], using the Chaloner Broad Energy Germanium (BEGe) detector manufactured by Mirion (Canberra) [35] with a nominal front face surface area of 50 cm^2, 30 mm length, and a measured relative efficiency of 48 %, for more details see [8]. For the analysis, secular equilibrium was assumed since the ^{40}K, ^{232}Th, and ^{238}U γ-rays are from the late sub-chains. Rock sample activities of LABChico and other laboratories are shown in table 5. Only statistical errors are shown, while systematic errors due to uncertainty in the rock composition can be of a few percent. Uncertainties reported in Boulby, Modane, Gran Sasso and SNOLAB vary from 5 to 22 %. Average values are reported for the SURF measurement with overall uncertainties estimated to be 10–20 %.

5 Geotechnical studies

A geotechnical study was performed to analyze the structural stability inside *La Guadalupe* mine. The following rock-mass characteristics were obtained: intact rock and discontinuities and an equilibrium limit analysis for the construction of the LABChico site. A three-dimensional model of the mine tunnel is shown in Fig. 1.

A three-dimensional mine model was built from a geographically referenced topographic survey with a fixed point, on the surface, belonging to the *Red Geodésica Nacional Pasiva*, Instituto Nacional de Estadística y Geografía (level bench 13038001) [36]. A total station (TS-09 Leica) [37] was used for the collection of the topographic data in conjunction with the MineSight mining design software [38] with which the three-dimensional model, shown in Fig. 1 was built through polygons. The specifications for the laboratory construction were simulated from this model, following the established geotechnical limits to ensure structural stability.

For the systematic geotechnical assessment and analysis, the tunnel of *La Guadalupe* mine was divided into stages, starting with the entrance (0 m) and finalizing at the selected site for the construction of the laboratory (150 m), labeled as (1) and (3) respectively in Fig. 1. The measured properties for the intact rock were density and Uniaxial Compressive Strength (UCS). These properties were obtained by on-site tests using a Schmidt hammer [39] and in the laboratory by Point Load Test (PLT), according to [40].

	^{40}K	^{232}Th	^{238}U
	Activity (Bq/kg)		
LABChico			
Rhyolite/Andesite	674.0 ± 2.0	24.0 ± 0.1	17.7 ± 0.2
SURF			
Rhyolite	1291.0	44.0	108.0
Boulby			
Halite	11.0	0.6	0.4
Mudstone	120.0	3.9	7.1
Modane			
Calcschist	182.0	10.2	11.8
Gran Sasso			
Dolomitic limestone	26.0	1.5	1.8
SNOLAB			
Norite	309.6	20.7	13.6

Table 5: Rock activity for different underground laboratories: LABChico, Boulby [17], Modane [20], Gran Sasso [16], SURF [22], and SNOLAB [14]. Only statistical errors are shown for LABChico. Uncertainties reported in Boulby, Modane, Gran Sasso, and SNOLAB vary from 5 to 22 %. Average values are reported for the SURF measurement and overall uncertainties are estimated to be 10–20 %.

The obtained rock discontinuity properties were: orientation, spacing, persistence, roughness, wall strength, aperture, filling, seepage, and block size according to [41]. Together with intact rock properties, the rock-mass quality was obtained according to the rock mass rating (RMR) [42, 43]. Such results represent the actual condition of the rock-mass along the tunnel and are the first approximation for the required artificial support for the excavation. The obtained rock-mass quality, for walls and roof, along stage 0 to 150 m have an RMR of III[†]. The rock mass quality index Q, ranges from 0.001 to 1000, and its classification goes from exceptionally poor to exceptionally good. The obtained Q value was in the classification *Fair* between 4 and 10 [43]. Also, the Marinos geological strength index (GSI) was obtained [44, 45], for the calculation of the rock-mass strength parameters: cohesion (C), friction angle, (ϕ) and Young modulus (Y) and the UCS of the rock−mass with the Hoek−Brown criteria [46], see Table 6. The limit equilibrium analysis and the wedge revision showed that the roof and the wall wedges, along with the LABChico site, have a safety factor (SF) greater than 1.5 (SF is the ratio of the available shear strength of the ground to that required to maintain equilibrium, and is recommended to be between 1.2 and 1.6) [47, 48]. For those regions which do not meet the sufficient safety conditions, the SF can be increased by modifying the excavation, reducing weight to the wedges and with a concrete cover in the perimeters, as shown in Fig. 8.

Stage 150	UCS	Y	C	ϕ
	MPa	MPa	MPa	Degrees
Walls	2.185	4016.53	0.243	66.41
Roof	4.855	7498.94	0.426	68.87

Table 6: Rock-mass strength parameters obtained with the Hoek-Brown criteria [46].

6 Conclusions

A 0.669 kg NaI detector was deployed 45 m away from the entrance of *La Guadalupe* mine to measure the γ-ray flux. The γ-ray background fluxes below 3 MeV and from ^{40}K(1.46 MeV) and ^{208}Tl(2.61 MeV) were calculated using an unfolding technique, for which the detector response matrix was computed via Monte Carlo simulations. The γ-ray flux in the energy range from 250 keV to 3 MeV is 0.1768 $\gamma/\text{cm}^2/\text{s}$. The flux from the ^{40}K, and ^{208}Tl γ-rays is 0.0363 ± 0.0020 $\gamma/\text{cm}^2/\text{s}$, and $0.0016 \pm 0.0005\,\gamma/\text{cm}^2/\text{s}$, respectively.

The measured flux in *La Guadalupe* mine was compared against other underground facilities such as SURF, SNOLAB, Boulby, Modane, and Gran Sasso. A rich potassium content is observed in rock samples from LABChico, as in SURF

[†]A RMR III has an average stand-up time of 1 week for 5 m span, a cohesion of rock mass between 0.2 and 0.3 MPa, an angle of internal friction of rock mass between 25 and 35 degrees, an allowable bearing pressure between 280 and 135 T/m^2 and a safe cut slope of 55 degrees [42]

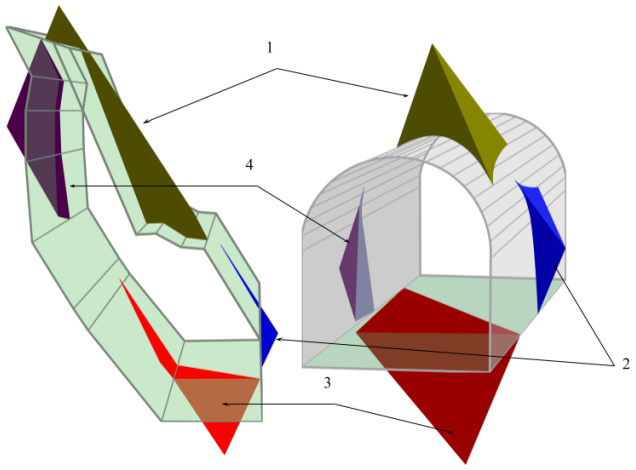

Figure 8: Limit equilibrium model at the selected site for the LABChico construction. Left, original excavation wedges. Right, projected wedges for the excavation. Label 1 indicates the roof wedge, 2 and 4 are the wall wedges and 3 the floor wedge (colors are used to differentiate the wedges).

and SNOLAB, resulting in a high γ-ray flux from ^{40}K. In contrast, a low γ-ray flux from ^{40}K is observed in Boulby, Modane, and Gran Sasso due to lower potassium content. The γ-ray assay performed to the mine rock sample indicates the presence of ^{40}K, ^{232}Th, ^{238}U isotopes with an activity of 674.0 ± 2.0 Bq/kg, 24.0 ± 0.1 Bq/kg, and 17.7 ± 0.2 Bq/kg, respectively.

The geotechnical studies performed in the tunnel, where the excavation for the LABChico site is projected, and on extracted rock samples, showed to have acceptable safety factors for the roof and the wall wedges. For those regions in which the safety factor needs improvement, amendments can be performed to reach the required structural stability.

The high energy γ-ray flux above 3 MeV will be measured in a future deployment of the NaI detector. The results presented in this manuscript will be valuable for gamma background modeling below 3 MeV to inform the design of shielding for low background counting experiments in LABChico.

Acknowledgements

This work is supported by the STFC Global Challenges Research Fund (Foundation Award, Grant ST/R002908/1) and the GCRF Translation Award EP/T015586/1. The authors also acknowledge support from DGAPA UNAM grants PAPIIT-IT100420 and PAPIIT-IN108020, and CONACyT grants CB-240666 and A1-S-8960. The authors thank Ejido El Puente and *La Guadalupe* mine local administration. The authors also thank Jaime Everardo Pérez and the machine shop at IF-UNAM.

References

1. A. Bettini. The world deep underground laboratories. *Eur. Phys. J. Plus*, 127:114, 2012.
2. Ian Lawson. Low Background Measurement Capabilities at SNOLAB. *J. Phys. Conf. Ser.*, 1342(1):012086, 2020.
3. J.L. Erchinger et al. Development of a low background liquid scintillation counter for a shallow underground laboratory. *Appl. Radiat. Isot.*, 105:209–218, 2015.
4. B.T. Cleveland, F.A. Duncan, I.T. Lawson, N.J.T. Smith, and E. Vazquez-Jauregui. Activities of gamma-ray emitting isotopes in rainwater from Greater Sudbury, Canada following the Fukushima incident. *Can. J. Phys.*, 90:599–603, 2012.
5. F. Ludwig, L. Wagner, and Al-Abdullah. The muon intensity in the Felsenkeller shallow underground laboratory. *Astropart. Phys.*, 112:24–34, 2019.
6. T. et al Szucs. Background in γ-ray detectors and carbon beam tests in the Felsenkeller shallow-underground accelerator laboratory. *Eur. Phys. J. A*, 55(10):174, 2019.
7. *Measurement of Radionuclides in Food and the Environment.* Number 295 in Technical Reports Series. International Atomic Energy Agency, Vienna, 1989.

8. P.R. Scovell et al. Low Background Gamma Spectroscopy at the Boulby Underground Laboratory. *Astropart. Phys.*, 97:160–173, 2018.
9. F. Piquemal. Modane underground laboratory: Status and project. *Eur. Phys. J. Plus*, 127, 2012.
10. L. Votano. The Gran Sasso Laboratory. *Eur. Phys. J. Plus*, 127, 2012.
11. N.J.T. Smith. The SNOLAB deep underground facility. *Eur. Phys. J. Plus*, 127, 2012.
12. K.T. Lesko. The Sanford Underground Research Facility at Homestake. *Eur. Phys. J. Plus*, 127, 2012.
13. X. Bertou. The ANDES underground laboratory. *Eur. Phys. J. Plus*, 127, 2012.
14. R. F. Perillo et. al. High energy gamma-rays measurements in the SNO cavity. *SNO-STR-97-009*, 1997.
15. K. J. Thomas. An estimate of the gamma flux in the east counting room of the davis cavern. *Davis Cavern, Technical Report, Lawrence Berkeley National Laboratory (LBNL)*, 2014.
16. J. Dorda D. Malczewski, J. Kisiel. Gamma background measurements in the Gran Sasso National Laboratory. *J Radioanal Nucl. Chem.*, 295:749–754, 2013.
17. Jan Kisiel Dariusz Malczewski and Jerzy Dorda. Gamma background measurements in the Boulby Underground Laboratory. *J Radioanal Nucl Chem.*, 293(3):1483–1489, 2013.
18. M. Haffke, L. Baudis, T. Bruch, A.D. Ferella, T. Marrodán Undagoitia, M. Schumann, Y.-F. Te, and A. van der Schaaf. Background measurements in the Gran Sasso underground laboratory. *Nuclear Instruments and Methods in Physics Research Section A: Accelerators, Spectrometers, Detectors and Associated Equipment*, 643(1):36–41, Jul 2011.
19. H. Ohsumi et al. Gamma-ray flux in the Frejus underground laboratory measured with NaI detector. *Nucl. Instrum. Meth.*, A482:832–839, 2002.
20. Jan Kisiel Dariusz Malczewski and Jerzy Dorda. Gamma background measurements in the Laboratoire Souterrain de Modane. *J Rad. Nucl. Chem.*, 292(2):751–756, 2012.
21. Xavier Bertou. The ANDES Deep Underground Laboratory. *PoS*, EDSU2018:027, 2018.
22. D. S. Akerib et al. Measurement of the Gamma Ray Background in the Davis Cavern at the Sanford Underground Research Facility. *Astropart. Phys.*, 116:102391, 2020.
23. A. M. Soreefan D. Falta M. Wall T. A. DeVol B. A. Powell, L. D. Hughes. Elevated concentrations of primordial radionuclides in sediments from the Reedy River and surrounding creeks in Simpsonville, South Carolina. *Journal of Environmental Radioactivity*, 94:121–128, 2007.
24. Canet C. et al. Cartografía geológica para la gestión del geopatrimonio y la planeación de rutas geoturísticas: aplicación en el geoparque mundial de la UNESCO Comarca Minera. 2017.
25. Cruz-Pérez M.A., Canet C., Salgado-Martínez E., Morelos-Rodríuez L., and García Alonso E. *Guía de Campo del Geoparque de la Comarca Minera.* 2018.
26. Scientific United Nations Educational and Cultural Organization. Statutes of the international geoscience and geoparks programme, UNESCO, 2015.
27. A. Aguilar-Arevalo et. al. Characterization of germanium detectors for the first underground laboratory in Mexico. *Journal of Instrumentation*, 15(11):P11014–P11014, nov 2020.
28. SDA38 – NaI(tl) scintillation detector. `http://www.spectrumtechniques.com/products/instruments/1-5-x-1-5-naitl-detector/`.
29. LLC Spectrum Techniques. Gamma disk sources, 2019. http://www.spectrumtechniques.com .
30. S. Agostinelli et. al. Geant4 a simulation toolkit. *Nuclear Instruments and Methods in Physics Research Section A: Accelerators, Spectrometers, Detectors and Associated Equipment*, 506(3):250 – 303, 2003.
31. S. Hauf et al. Validation of Geant4-based radioactive decay simulation. *IEEE Transactions on Nuclear Science*, 60:2984–2997, Aug 2013.
32. Rene Brun and Fons Rademakers. ROOT an object oriented data analysis framework. *Nuclear Instruments and Methods in Physics Research Section A: Accelerators, Spectrometers, Detectors and Associated Equipment*, 389(1):81 – 86, 1997. New Computing Techniques in Physics Research V.
33. National Laboratory Henri Becquerel. Nuclear and atomic data, 2019. `http://www.lnhb.fr/nuclear-data/nuclear-data-table/`.
34. Drew Anthony Fustin. *First Dark Matter Limits from the Coupp 4kg Bubble Chamber at a Deep Underground Site.* PhD thesis, The University of Chicago, 3 2012.
35. Mirion, 2020. `http://www.gammadata.se/assets/Uploads/BEGe-SS-C49318.pdf`.
36. Instituto Nacional de Estadística y Geografía. Red geodésica nacional pasiva, 2020. `https://www.inegi.org.mx/temas/rgnp_integrada/`.
37. Leica flexline ts 09 plus. `https://leica-geosystems.com`.
38. Minetec. Minesight software solutions from mintec, 2020. `http://www.minesight.com/`.
39. International Society for Rock Mechanics. Suggested method for determination of the Schmidt rebounds hardness. 2014.
40. International Society for Rock Mechanics. Suggested method for determining point load strength. 1985.

41. International Society for Rock Mechanics. Suggested method for the quantitative description of discontinuities in rock masses. 1978.
42. *Engineering Rock Mass Classifications*. John Wiley and Sons, 1989.
43. N. Barton, R. Lien, and J. Lunde. Engineering classification of rock masses for the design of tunnel support. *Rock mechanics*, 6(4), 1974.
44. V. Marinos, Marinos P., and E. Hoek. The GSI: Applications and limitations. *Bulletin of Engineering Geology and the Environment*, 64:55–65, 2005.
45. E. Hoek and P. Marinos. Predicting tunnel squeezing problems in weak heterogeneous rock masses. *Tunnels and Tunneling International*, 1-2, 2000.
46. E. Hoek and E.T. Brown. The Hoek-Brown failure criterion and GSI. *Journal of Rock Mechanics and Geotechnical Engineering*, 11(3):445 – 463, 2019.
47. B. Trak. How Safe is the "Factor of Safety" Concept in Geotechnical Practice. *Geo-Risk*, 285, 2017.
48. A. W. Bishop. The use of the slip circle in the stability analysisi of slopes. *First Tech. Sess.: General Theory of Stability of Slopes*, 1954.